# Micromagnetic simulations for improving thermal stability of magnetic skyrmions

Mackenzie Geckler
*Center for Emergent Materials, The Ohio State University*
*July 24, 2020*

## ABSTRACT

Magnetic skyrmions are vortex-like chiral topological spin textures that arise in magnetic materials due to the competition between the Dzyaloshinskii-Moriya interaction (DMI) and exchange interaction. Skyrmions have potential applications as carriers in high-density information storage and transfer in the future. This project investigates how DMI strength and exchange interaction strength affect the thermal stability of skyrmions. To answer this question, MuMax[3] micromagnetic simulation program is first verified using a standard micromagnetics problem, then used to test the thermal stability of skyrmions in TmIG/Pt. Results show that skyrmions can evolve from the helical phase when temperature is increased, and this evolution occurs at higher temperatures for greater DMI strengths. Skyrmion $T_c$ also increases with greater exchange interaction strength.

## I. Introduction and Background

Magnetic skyrmions are vortex-like topological spin texture in magnetic materials that arise due to competing effects from the Dzyaloshinskii-Moriya interaction (DMI) and exchange interaction. They are of interest due to their potential use in memory and logic applications as carriers in high density information transfer[1]. Skyrmions are good candidates for this type of application due to their nanoscale size, high current density, tunability to fields, stability, and ability to be moved through materials when driven by current[1,2].

There are two types of skyrmions: Bloch and Néel. Both arise from separate types of DMI, with Bloch having bulk DMI and Néel having interfacial DMI. To create the needed interfacial DMI to stabilize Néel skyrmions, the interface of thin film ferromagnets and strong spin-orbit coupling (SOC) non-magnetic metals are commonly used, as seen in Figure 1a. When the ferromagnet becomes sufficiently thin, interfacial DMI can create an environment for skyrmions[2]. In ordinary magnetic materials, the

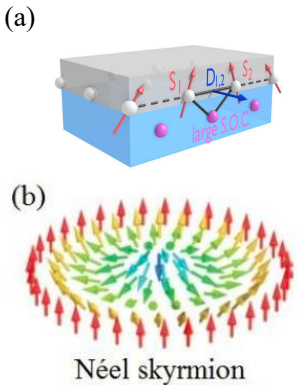


**Figure 1.** Overview of skyrmion behavior: (a) DMI between neighboring spins at interface of large SOC materials and thin ferromagnet (from Reference 3); (b) magnetization configuration of a Néel skyrmion (from Reference 4).

magnetic exchange interaction leads to alignment of neighboring spins collinearly, which is due to the dot product of the neighboring spin vectors in the exchange (Heisenberg) Hamiltonian:

$$\mathcal{H}_{Heis} = -\sum_{i,j} J\langle \vec{S}_i \cdot \vec{S}_j \rangle \quad [1]$$

However, in materials with broken inversion symmetry it becomes energetically favorable to

break the symmetry of neighboring aligned spins, which can be seen in the cross-product term of the DMI Hamiltonian:

$$\mathcal{H}_{\mathrm{DMI}} = -\sum_{<i,j>} \vec{D}_{ij} \cdot [\vec{S}_i \times \vec{S}_j] \quad [2]$$

To minimize the energy, the cross-product between neighboring spins must be maximized, which occurs when spins are angled 90 degrees from each other. The competition between the exchange interaction wanting to align spins and the DMI wanting to angle spins 90 degrees apart gives rise to skyrmions in magnetic materials.

Skyrmions were first observed and studied at low temperatures, because high temperatures tend to deform their shape and create fluctuations in size[5]. However, skyrmions that can survive at higher temperatures are highly desirable because cryogenic conditions are difficult to maintain and not efficient for storing and transforming information. Kovalev, A. & Sandhoefner, S. discuss materials skyrmions have been commonly studied in at both low and high temperatures. At low temperatures, skyrmions can be found in Fe and PdFe layers on Ir[6]. To create skyrmions at high temperatures, often stacking of magnetic and non-magnetic layers is used to create an additive interfacial DMI, such as in Co layered between two non-magnetic layers such as Ir and Pt[6].

Several descriptions of skyrmion behavior over various temperatures have been studied. In Montoya, S. A. et al., studies of Fe/Gd multilayer slabs at various temperatures ranging from 50 to 300 Kelvin were studied both in the lab using resonant soft X-ray scattering, Lorentz transmission electron microscopy, transmission X-ray microscopy and via micromagnetic simulations[7]. A skyrmion lattice appeared within a range near room temperature for 0.34nm Fe and 0.4nm Gd at 2.0-2.5 T magnetic field, and at a slightly lower temperature for 0.36nm Fe and 0.4nm Gd[7]. This paper and others confirm the existence of skyrmions at room temperature as well as other nonzero temperatures, which is key to the development of skyrmions as useful tools for information transfer and storage in the future.

This project uses micromagnetic simulations to study the effect of changing DMI and exchange interaction strength on the thermal stability of Néel skyrmions in TmIG/Pt. Phase diagrams depicting temperature-dependent behavior of skyrmions have applications in the future for finer calibration of parameters to study skyrmions in both laboratory and simulated environments.

## II. Methods

### *A. Landau-Lifshitz-Gilbert equation*

The Landau-Lifshitz-Gilbert (LLG) equation

$$\frac{d\mathbf{M}}{dt} = -\gamma \left( \mathbf{M} \times \mathbf{H}_{\mathrm{eff}} - \eta \mathbf{M} \times \frac{d\mathbf{M}}{dt} \right) \quad [3]$$

describes the damped precession of magnetization in a magnetic solid. It is used in micromagnetics to describe the time evolution of the magnetization of a ferromagnet within a magnetic field. Ferromagnets are magnetic materials that can have non-zero magnetization even in the absence of an applied magnetic field. The left side of the LLG equation is the time derivative of the magnetization, or the torque. The first term on the right side describes the magnetization precession around the effective magnetic field ($H_{eff}$) and is the Landau-Lifshitz torque. The second term on the right side is the Gilbert damping term, which describes the damping of the precession of magnetization around the effective magnetic field. Gilbert proposed an alternate damping term that depends on time derivative of the magnetization which better represents ferromagnets where damping is large. In the LLG equation, $\gamma$ is the electron gyromagnetic ratio and $\eta$ is the damping parameter, which is a characteristic of the material.

The LLG equation is often solved numerically in simulations due to its complex analytical solution. To solve analytically, the backward difference method in Cartesian coordinates can be used with magnetization held as independent variable[8].

### *B. Verification of MuMax³*

MuMax³ is a GPU-accelerated micromagnetic simulation software[9] used throughout this project as a tool for simulations. MuMax³ calculates magnetization of given materials by discretizing the materials into small volumes and solving the LLG equation numerically in each volume, a method called the finite element method. Then MuMax³ can return magnetization of the material, as well as the values of other parameters, for each time step.

First, I performed a verification of MuMax³ using a standard micromagnetics problem: calculating the relationship between magnetization angle and strength of an external applied field in a thin film. In this problem I assumed only the external applied field and demagnetizing field contributed to the magnetization angle in the film. This problem was solved both analytically and numerically and results were compared to ensure the accuracy and understand the use of MuMax³ for micromagnetic simulations. A visual schematic of the problem is shown in Figure 2.

Derivation of the magnetization angle as a function of strength and angle of incidence of the applied external field was done, starting with the LLG equation and the condition for thermodynamic equilibrium. Spin dynamics is described with

$$-\frac{1}{\gamma}\frac{d\boldsymbol{M}}{dt} = \boldsymbol{M} \times \boldsymbol{H}_{eff} \qquad [4]$$

And in thermodynamic equilibrium

$$\frac{d\mathrm{M}}{dt} = 0 \qquad [5]$$

So therefore

$$\mathrm{M} \| \mathrm{H}_{\mathrm{eff}} \qquad [6]$$

is the ground state configuration of the magnetization. From the LLG equation, I calculated the equation for $\mathbf{H_{eff}}$ using only the external applied field and demagnetizing field components as

$$\boldsymbol{H_{eff}} = \boldsymbol{H_D} + \boldsymbol{H_{ext}} \qquad [7]$$

Demagnetizing field can be calculated using the tensor form for a uniformly magnetized ellipsoid as

$$\mathrm{H}_D = -\begin{pmatrix} N_{xx} & 0 & 0 \\ 0 & N_{yy} & 0 \\ 0 & 0 & N_{zz} \end{pmatrix} \mathrm{M} \qquad [8]$$

Where $N_x$,$N_y$, and $N_z$ are the demagnetizing factors and **M** is the saturation magnetization. For an infinite thin film in the xy plane, $N_x = N_y = 0$ and $N_z = 4\pi$. so

$$\boldsymbol{H_D} = 4\pi M_s \sin(\varphi)\,\hat{\mathbf{k}} \qquad [9]$$

where $\sin(\varphi)$ takes the z component of the magnetization and $\varphi$ is the magnetization angle. If the external field is applied in the yz plane, then

$$\boldsymbol{H_{ext}} = |H_{ext}|\cos(\theta)\,\hat{\jmath} + |H_{ext}|\sin(\theta)\,\hat{\mathbf{k}} \qquad [10]$$

where $\theta$ is the angle the external field makes with the film. Therefore,

$$\boldsymbol{H_{eff}} = |H_{ext}|\cos(\theta)\,\hat{\jmath} + |H_{ext}|\sin(\theta)\,\hat{\mathbf{k}} - 4\pi M_s \sin(\varphi)\,\hat{\mathbf{k}} \qquad [11]$$

Taking the ground state parallel configuration equation [6] into account, I can then write

$$\frac{\sin(\varphi)}{\cos(\varphi)} = \frac{|H_{ext}|\sin(\theta) - 4\pi M_s \sin(\varphi)}{|H_{ext}|\cos(\theta)} \qquad [12]$$

as the relationship between magnetization and effective field. I then compared this result to numerical solutions using Mumax³.

The simulations were run for three values of $4\pi M_s$, where $M_s$ is the saturation magnetization of the film, and for various angles of applied external field. From these results, we can see that the analytical equation derivation and numerical solution via MuMax³ to this problem

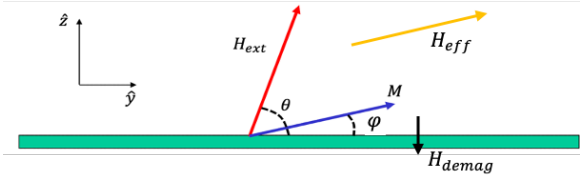


**Figure 2.** Visual depiction of thin film magnetization angle problem. Magnetization angle is given as $\varphi$.

agree. Looking at similar graphs for $4\pi M_s = 100\ G$ and 1 Tesla, we can also conclude that as the magnitude of the external applied field becomes much greater than $4\pi M_s$, a larger external field must be applied to pull the magnetization to its final angle.

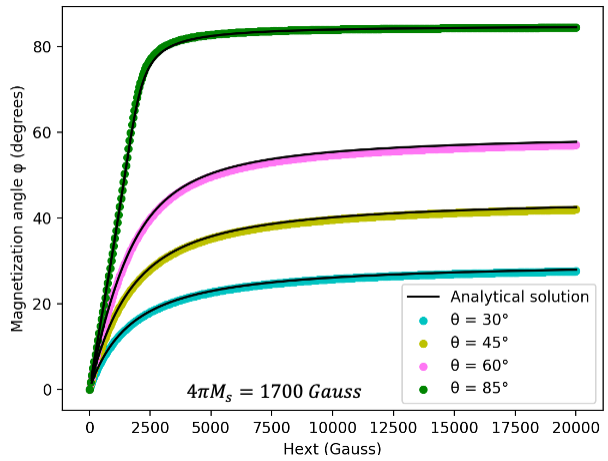


**Figure 3.** Numerical verification results of standard micromagnetics thin film magnetization angle problem in MuMax³. Plot shows numerical solution obtained in MuMax³ graphed with numerically solved analytical solution of Equation [12] for $4\pi M_s = 1700\ G$ for several angles of external field with plane.

### *C. Skyrmion modeling in MuMax³*

To accurately study the behavior of skyrmions at various temperatures, I first created a phase diagram of skyrmion behavior over the parameters uniaxial anisotropy, $K_u$, and external field strength, $B_{ext}$, following research of Shao, Q. & Liu, Y. et al. to ensure my simulations were running as expected[10]. To create skyrmions in MuMax³, I set a random magnetization in TmIG/Pt and let it decay for 10ns to reach its ground state. A depiction of the process to obtain skyrmions in MuMax³ is shown in Figure 4. I obtained a phase diagram for external field and uniaxial anisotropy shown in Figure 5. I used the following parameters in the creation of this phase diagram over various external fields and anisotropy constants:

Saturation magnetization ($M_s$)= 50 kA/m
DMI (D) = 50 $\frac{\mu J}{m^2}$
Exchange strength (A) = 0.8 pJ/m
Temperature (T) = 0 K

My phase diagram verifies results from Shao, Q. & Liu, Y. et al. as the expected phases for each value of anisotropy and external field appear. A skyrmion lattice appears at 0.05 T and $K_u = -\frac{D^2}{2A}$, which is expected from Shao & Liu, et al.'s phase diagram. The predicted skyrmion phase, combined phase (skyrmion and helical), and magnetization oriented completely in the direction of external field arise at the expected values of external field strength and uniaxial anisotropy.

To study behavior of skyrmions under increasing thermal fluctuations, I introduced temperature as an additional field that fluctuates and whose magnitude is equivalent to the temperature I want to apply. I created a sweep over this temperature field from 0 K to 100 K in steps of 10 K and simulated this sweep for a 5nm by 5nm by 3nm slice of TmIG/Pt with a grid size of (200, 200, 1). I tested three different values of DMI strength and exchange interaction strength for their interesting effects on skyrmion thermal stability. I also tested four additional values of DMI strength, exchange interaction strength, and saturation magnetization for verification of skyrmion behavior on larger scales of these parameter ranges.

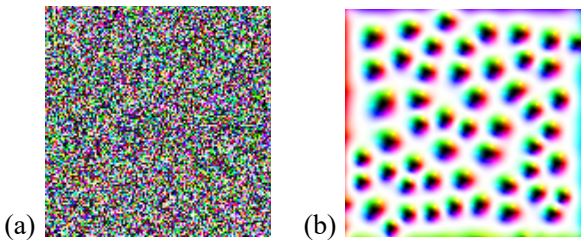


**Figure 4.** Image of (a) random magnetization in MuMax³ that relaxes into (b) skyrmions in MuMax³.

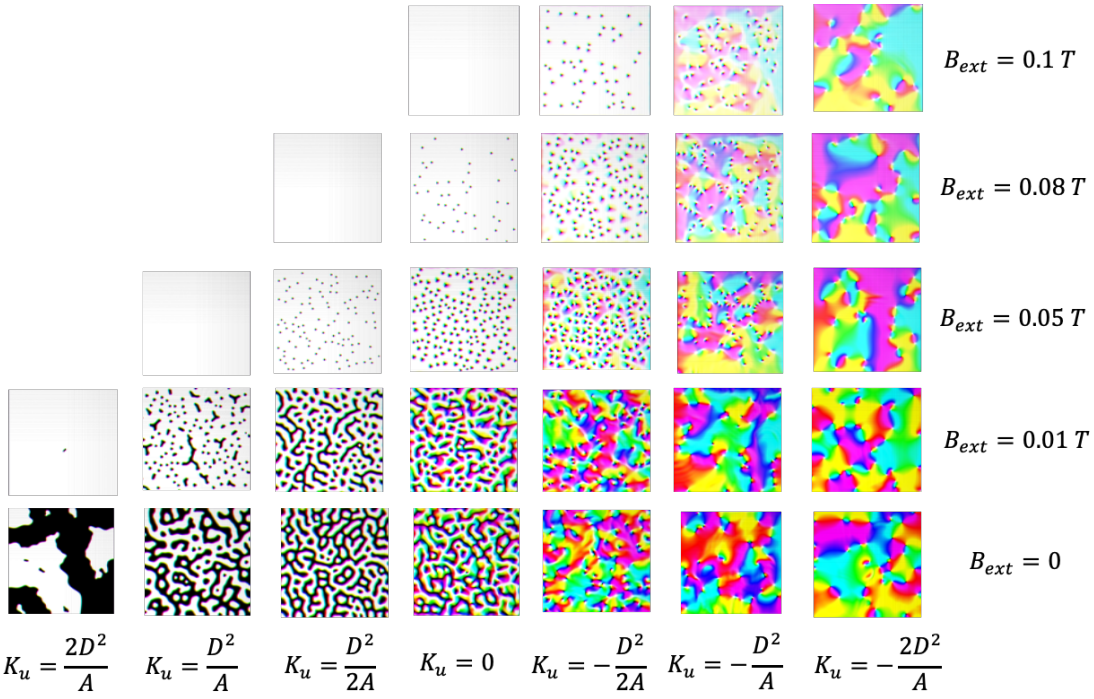


**Figure 5.** Skyrmion phase diagram for various values of anisotropy $K_u$ and external applied field $B_{ext}$. Results agree with Shao & Liu et al. and show skyrmion lattice phase, isolated skyrmions phase, stripe phase, and combination phases.

## III. Results and Discussion

Results for my phase diagrams are shown in Figure 6 for three values of DMI and exchange interaction strength. These rows are were chosen to study interesting characteristics and phenomena related to the two parameters.

Also included in Figure 7 are phase diagrams over larger spans of DMI and exchange interaction strength, as well as saturation magnetization, to verify the expected changes to skyrmion behavior at more extreme values of these parameters. These graphs demonstrate expected behavior of skyrmions at a wider range of values for each parameter and were used to narrow the scope of the final phase diagrams to a range of interest. Rows corresponding to DMI = 50 $\mu$J/m$^3$, Aex = $8 \cdot 10^{-13}$ J/m, and $M_S$ = 50,000 A/m are identical because those values were used as the base for each respective parameter when that parameter was not being studied.

The phase diagram for DMI strength, Figure 6a, shows three values (0.11 - 0.13 mJ/m$^3$) that create a combined phase of helical and skyrmion phase in TmIG/Pt at 10 K. After increasing the temperature to 100 K, many of the helical stripes are no longer visible. Circles around some of the helical stripes in the phase diagram help demonstrate stripes that become skyrmions when temperature is increased. Increasing the DMI strength appears to increase the temperature needed to change the helical phase stripes into skyrmions. DMI strength of 0.13 mJ/m$^3$ retains more of its helical phase at 100 K, where many stripes in 0.12 and 0.11 mJ/m$^3$ DMI strength disappear around 30-70 K.

Figure 6b shows the phase diagram over exchange interaction strength and temperature. Exchange interaction strength is varied from 2.0 - 4.0 $\cdot$ $10^{-13}$ J/m and temperature is shown between 10 and 100 K. From this phase diagram, critical temperature, $T_c$, at which skyrmions are no longer visible in the material can be obtained. $T_c$ increases as the strength of exchange interaction is increased. For $2.0 \cdot 10^{-13}$ J/m, $T_c$ occurs at 70 K, but at $3.0 \cdot 10^{-13}$, $T_c$ occurs around 100 K. Critical temperature is not

reached in this phase diagram for $4.0 \cdot 10^{-13}$, meaning its $T_c$ is above 100 K, which is expected from the proposed relationship.

There are important implications of the relationships discovered in these phase diagrams. The ability to convert helical phase stripes into skyrmions at higher temperatures could be useful for both experimental and theoretical researchers studying skyrmions in the future. The ability to create skyrmions out of other phases when thermal fluctuations are

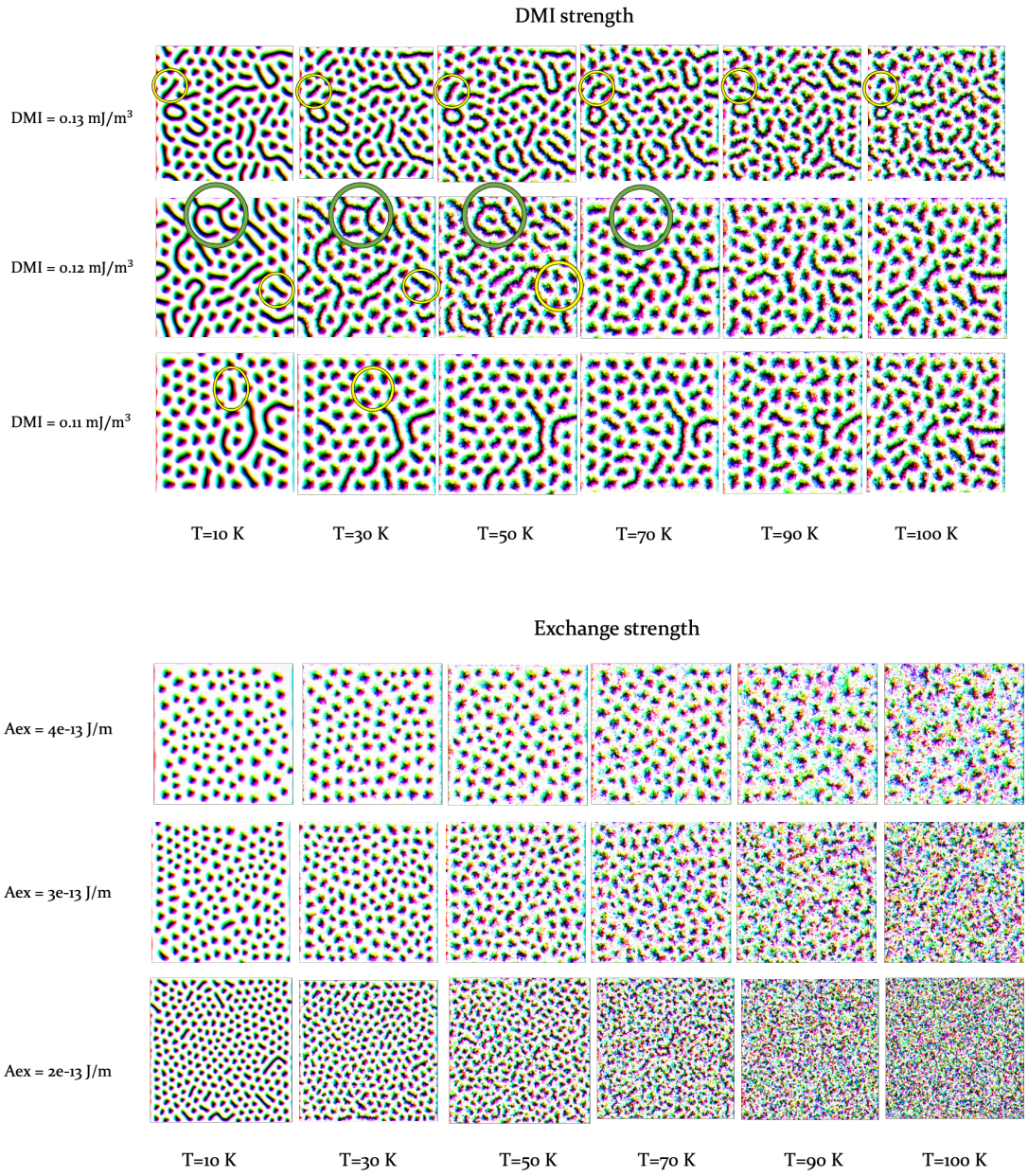


**Figure 6.** Phase diagrams over temperature and (a) DMI strength, (b) exchange interaction strength for skyrmions modeled using the additional parameters described in Methods. Circles in (a) indicate small helical phases that become skyrmions at a certain temperature.

applied could be useful for large scale studies of skyrmions and to create more carriers in high density information storage and transfer. Next steps would be to identify the theory behind this transition and experimentally observe this phenomenon in a thin film ferromagnet.

Understanding the critical temperature above which skyrmions do not exist in the material is important to understand for

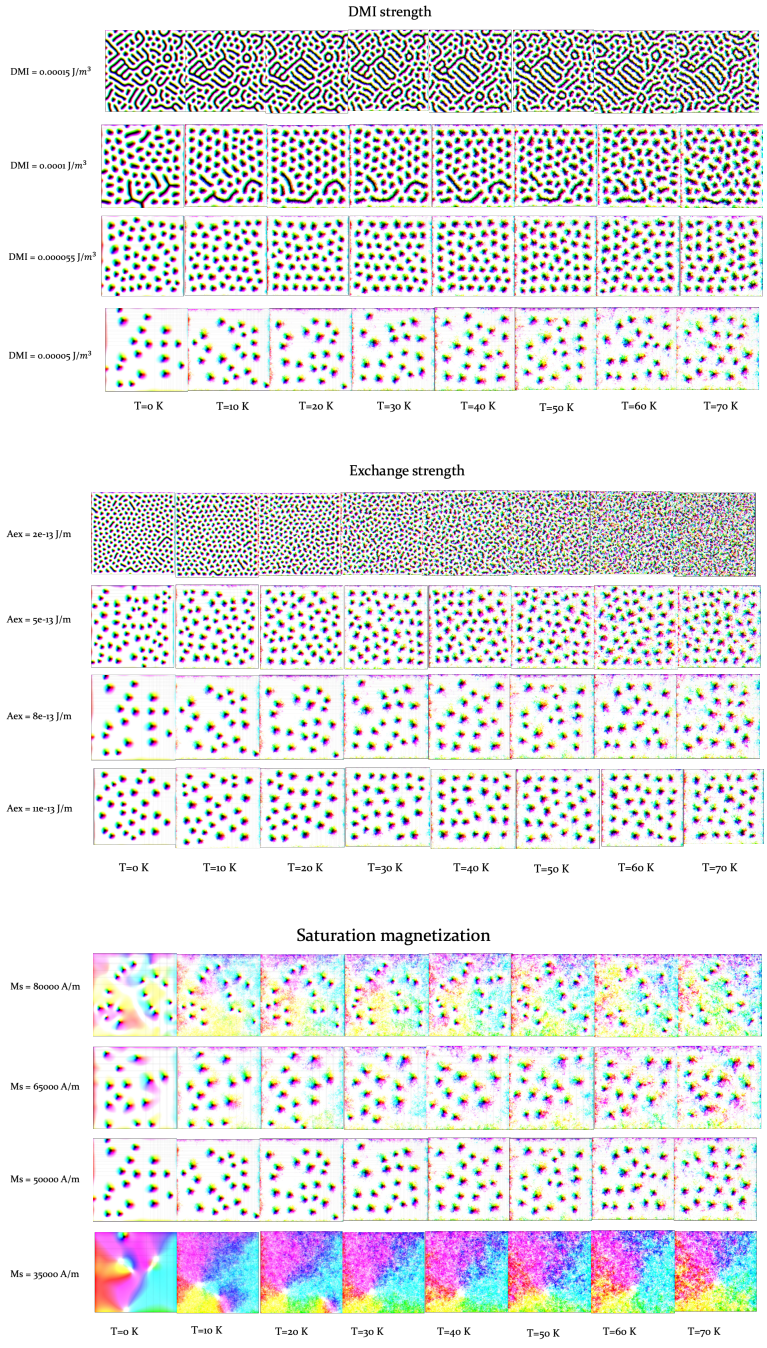


**Figure 7.** Phase diagrams showing skyrmion behavior on larger ranges of (a) DMI strength; (b) exchange interaction strength; and (c) saturation magnetization. These diagrams agree with known behavior of skyrmions for larger ranges of these parameters and serve to narrow the range of parameters for further study.

experimental studies and future applications of skyrmions. Materials must be maintained below this critical temperature to effectively study skyrmions and use them as information carriers. Significant research is being done and should continue to be done to improve this critical temperature so skyrmions can be used and studied closer to room temperature in a variety of applicable materials.

## IV. Conclusions

This project verified MuMax[3] micromagnetics simulation program for the use of modeling skyrmions in magnetic materials. During this project, I obtained relationships between skyrmion behavior and the introduction of thermal fluctuations in TmIG/Pt. I identified a relationship between exchange interaction strength and critical temperature, $T_c$, at which skyrmions disappear. I also observed that increasing DMI strength gave rise to the conversion of helical phase stripes to skyrmions at an increasing temperature threshold as DMI strength increased. Future work should experimentally verify these results and verify analytical expressions for these relationships derived from theory.

## V. Acknowledgments

I would like to thank Dr. P. Chris Hammel, Dr. Denis Pelekhov, and Dr. Mohit Randeria, as well as Jacob Freyermuth, Guanzhong Wu, and Po-Kuan Wu for advising and supporting my research experience this summer.

This REU program is part of an NSF Materials Research Science and Engineering Center (MRSEC) supported under NSF Award Number DMR-1420451.

## VI. Footnotes, Endnotes and References

1. Wang, X.S., Yuan, H.Y. & Wang, X.R. A theory on skyrmion size. *Commun Phys* **1**, 31 (2018).

2. Tomasello, R. et al. Origin of temperature and field dependence of magnetic skyrmion size in ultrathin nanodots. *Phys. Rev. B* **97**, 060402(R) (2018).

3. Cros, V. et al. Individual skyrmions at room temperature: From magnetic thin films to magnetic multilayers**.** *SOCSIS Greece*, (2015).

4. Medlej, I. & El Haj Hassan, F. (2019). Micromagnetic modeling of skyrmion dynamics and THz oscillation in antiferromagnets. 10.13140/RG.2.2.17326.66889.

5. Marrows, C.H. An inside view of magnetic skyrmions. *Physics* **8**, 40 (2015).

6. Kovalev, A.A. & Sandhoefner, S. Skyrmions and antiskyrmions in quasi-two-dimensional magnets. *Frontiers in Physics* **6** (2018): 98.

7. Montoya, S.A. et al. Tailoring magnetic energies to form dipole skyrmions and skyrmion lattices, *Physical Review B*, **95** (2017).

8. Nakatani, Y. et al. Direct Solution of the Landau-Lifshitz-Gilbert Equation for Micromagnetics. *Jpn. J. Appl. Phys.* **28** 2485 (1989).

9. Vansteenkiste, A. et al. The design and verification of mumax3. *AIP Advances* **4**, 107133 (2014).

10. Shao, Q. & Liu, Y. et al. Topological Hall Effect at Above Room Temperature in Heterostructures Composed of a Magnetic Insulator and a Heavy Metal. *Nature Electronics* **2.5** (2019): 182–186.